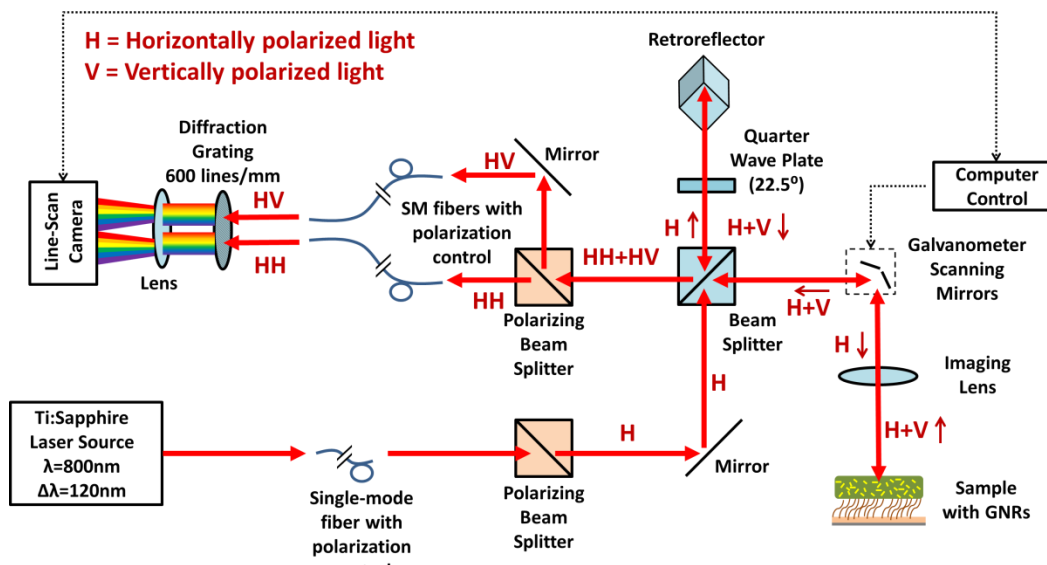**SUPPLEMENTAL SECTION**

Fig. S1 – Diagram of OCT system used in this study.

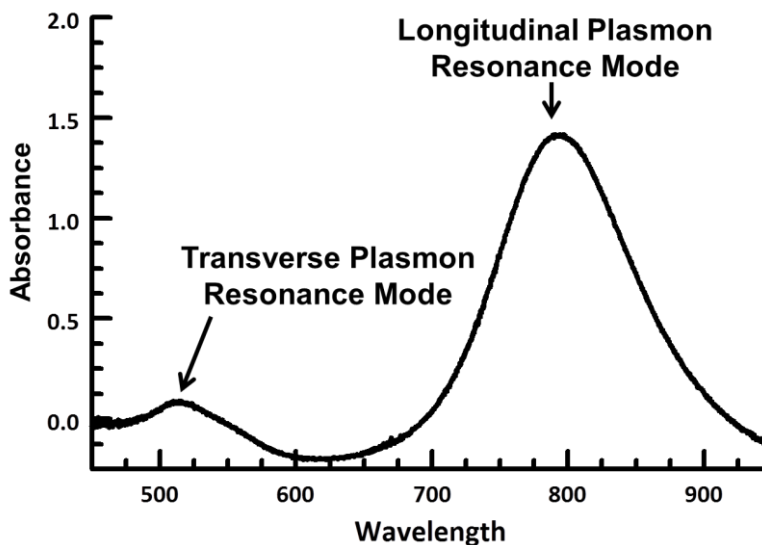**Fig. S2** –Extinction spectrum of GNRs where absorbance=-ln(T), with T=transmittance (density is ~1×10^{7} GNRs/µL in a 1 cm thick sample).
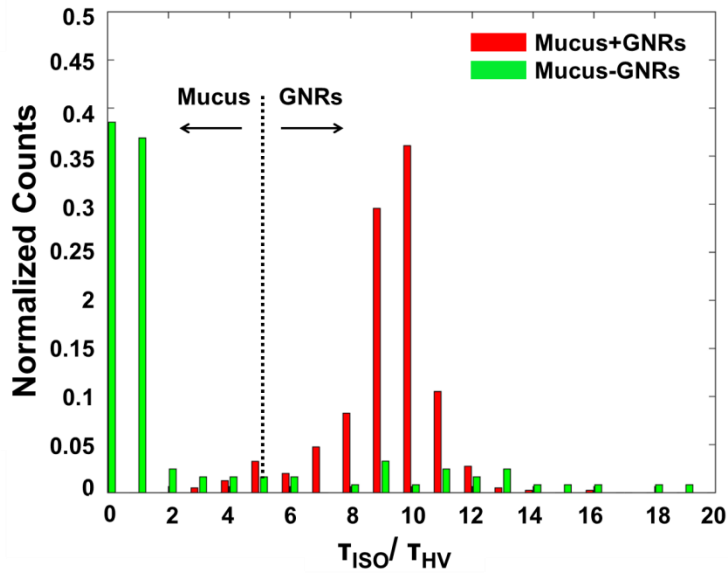
Fig. S3 – Normalized histogram of the ratio of the isotropic and cross-polarized decorrelation times, showing that the ratio is around 1 (with 0 indicating no real decay constant) for only mucus and centering around 9-10 for mucus with GNRs. We therefore chose to use 5 as the cut-off point for the DS-OCT signal test.
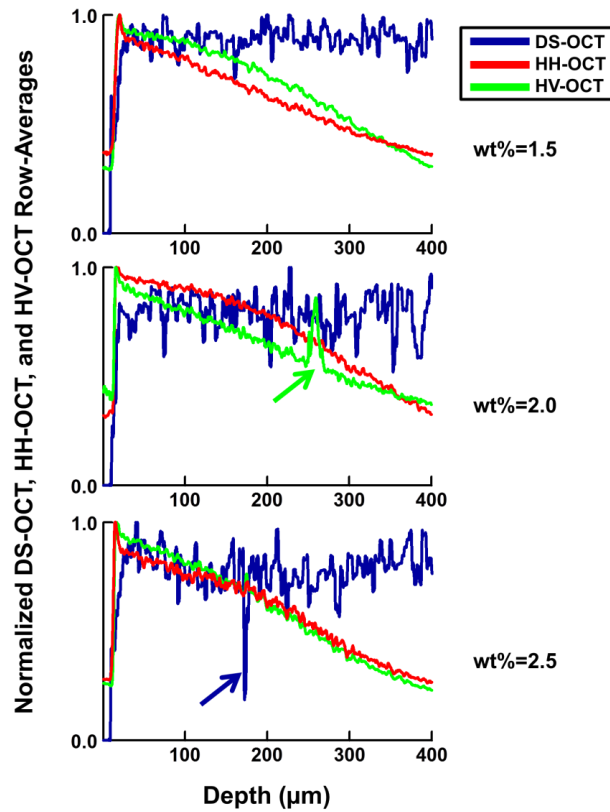

Fig. S4 – OCT signals versus mucus depth. Plots are normalized averages of values over time in DS-, HH-, and HV-OCT images for 1.5%, 2.0%, and 2.5% mucus concentrations in *ex vivo* stationary mucus reported in Fig. 1a. These plots illustrate the independence of GNR diffusion and HH/HV intensities, and the independence of diffusion measurements with mucus depth. Green arrow: A spike in HV intensity does not appear to affect the trend in wt% measured. Blue arrow: A dip in DS-OCT signal (wt%) of mucus at ~180 μm depth does not appear to be influenced by HH/HV intensities at the same location.

Monte Carlo simulations were performed to verify the ability to accurately quantify the translational diffusion rate via DS-OCT. The Brownian motion of $n=15$ particles per coherence volume was simulated by seeding an axial window of 3 coherence volumes with random initial particle positions, then advancing particle motion in time by adding a Gaussian random variable of zero mean and standard deviation $= (2 D_T \Delta t)^{1/2}$, where Δt is the sampling time, over $N=4000$ samples as in our lab experiments. The resultant electric field backscattered from the particles was simulated by coherently summing $\exp(-i\, q\, z_j(t))*\exp(-z_j(t)^2/l_c^2)$ over all $j=1\ldots n$ particles, where $q = 4\pi/\lambda$ is the scattering vector, l_c is the coherence length, and each particle was assumed to have equal backscattering coefficient. Since our coherence volume is ~5× shorter axially than laterally, and total particle displacement over the measurement time is already relatively small compared to the coherence length, lateral motion was not simulated. The procedure was repeated 3 times to simulate the 3 axial positions that are averaged in our lab experiments. At this point, the same processing method was used as in our experimental workflow, resulting in an estimated value of the decay constant $\tau_{1/e}$, which was compared to the theoretical decay constant given by the D_T used in the simulation. Finally, the whole procedure was repeated 10 times to obtain a mean and standard deviation of the $\tau_{1/e}$ estimate, while the "true" simulated $\tau_{1/e}$ was stepped over 20 values as shown in Fig. S5. While rotational motion was not simulated, it is expected that the general trends in estimation for a random process that decorrelates with a characteristic time of $\tau_{1/e}$ will be similar to that for translational diffusion.

The results shown in Figures S5 and S6 indicate that the procedures used produce a reasonable estimate of the speckle fluctuation decay constant over a range of $\tau_{1/e}$ values that lie between the sampling time ($\Delta t=1$) and the total imaging time ($T_{tot} = N\,\Delta t = 4000$). Specifically, over the range of $\tau_{1/e}$ values in our test used in Eq. (8), the error in the estimates lie between 10% at $\tau_{1/e} = f\,/\,3.25$ and -35% at $\tau_{1/e} = n_A\,/\,10.75\,f$. Interestingly, there is a reproducible positive bias in $\tau_{1/e}$ at shorter $\tau_{1/e}$, and negative bias in $\tau_{1/e}$ at longer $\tau_{1/e}$. Further effort is needed to better understand the mechanism for these biases, and to correct for them to increase the accuracy and dynamic range of DS-OCT. Importantly, these biases do not affect the work in this paper on quantifying mucus *wt*%, because a calibration curve is established initially to relate D_T measurements (including these biases) with *wt*%. Furthermore, our data was collected using carefully chosen sampling rates such that $\tau_{1/e}$ was well-centered within the dynamic range of Eq. (8) where the estimation error is minimal.
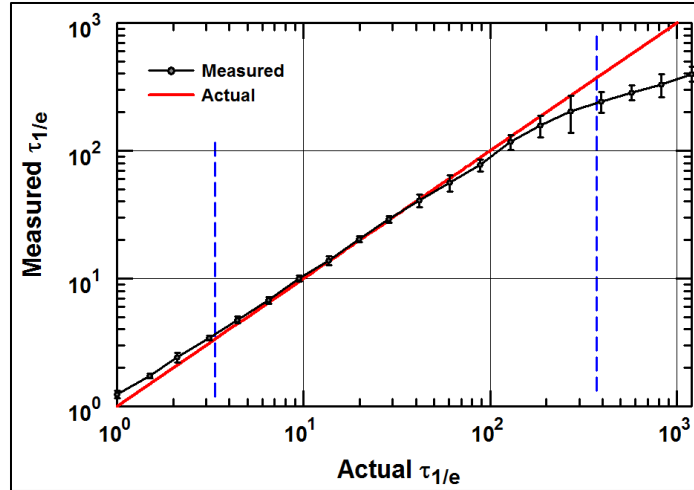
Fig. S5. Results of Monte Carlo Simulations of DS-OCT measurements showing how the measured decay constant ($\tau_{1/e}$) varies with the true decay constant. All times are reported relative to the sampling time ($\Delta t=1$). Blue dashed lines indicate the minimum and maximum $\tau_{1/e}$ accepted by the test in Eq. (8). (Mean ± standard deviation over 10 simulated measurements).
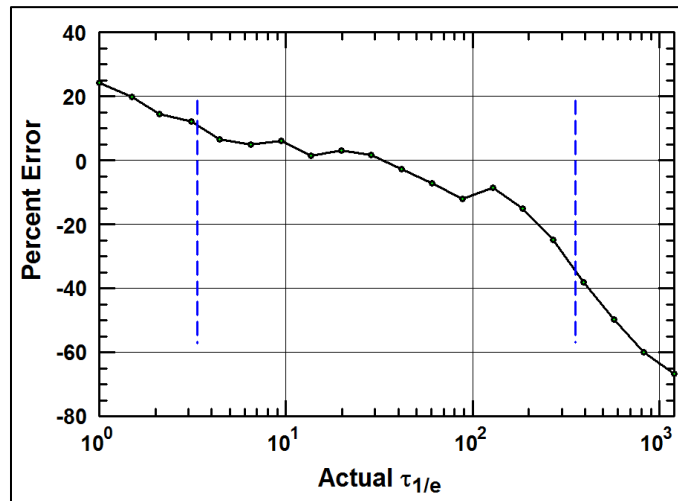

Fig. S6. Percent error in estimated $\tau_{1/e}$ according to Monte Carlo Simulations. Blue dashed lines indicate the minimum and maximum $\tau_{1/e}$ accepted by the test in Eq. 8.

Vid. S1 – HH-OCT timelapse imaging of endogenous HBEC mucus without GNRs transporting on an MCTD. Video dimensions are 2.3×3.0 mm ($x \times z$) and display is at 9× speed.

Vid. S2 – HH-OCT timelapse imaging of IS treatment on an HBEC over 4.5 min. Video dimensions are 2.3×3.0 mm ($x \times z$) and display is at 10× speed.

Vid. S3 – HH-OCT timelapse imaging of HS treatment on an HBEC over 4.5 min. Video dimensions are 2.3×3.0 mm ($x \times z$) and display is at 10× speed.